

Deciphering fluid flow at the magmatic-hydrothermal transition: A case study from the world-class Panasqueira W–Sn–(Cu) ore deposit (Portugal)

Gaëtan Launay, Stanislas Sizaret, Laurent Guillou-Frottier, Eric Gloaguen, Filipe Pinto

▶ **To cite this version:**

Gaëtan Launay, Stanislas Sizaret, Laurent Guillou-Frottier, Eric Gloaguen, Filipe Pinto. Deciphering fluid flow at the magmatic-hydrothermal transition: A case study from the world-class Panasqueira W–Sn–(Cu) ore deposit (Portugal). Earth and Planetary Science Letters, 2018, 499, pp.1-12. 10.1016/j.epsl.2018.07.012 . hal-01955965

HAL Id: hal-01955965
https://brgm.hal.science/hal-01955965

Submitted on 14 Dec 2018

HAL is a multi-disciplinary open access archive for the deposit and dissemination of scientific research documents, whether they are published or not. The documents may come from teaching and research institutions in France or abroad, or from public or private research centers.

L'archive ouverte pluridisciplinaire **HAL**, est destinée au dépôt et à la diffusion de documents scientifiques de niveau recherche, publiés ou non, émanant des établissements d'enseignement et de recherche français ou étrangers, des laboratoires publics ou privés.



Distributed under a Creative Commons Attribution - NonCommercial - NoDerivatives 4.0 International License

Deciphering fluid flow at the magmatic-hydrothermal transition: a case study from the world-class W-Sn-(Cu) ore deposit of Panasqueira (Portugal)

Gaëtan Launay[1,2], Stanislas Sizaret[1], Laurent Guillou-Frottier[1,2], Eric Gloaguen[1,2] and Filipe Pinto[3,4]

(1) ISTO, UMR7327, Université d'Orléans, CNRS, BRGM, F-45071 Orléans, France

(2) BRGM, F-45060 Orléans, France

(3) Beralt Tin & Wolfram, S.A., Geology Department, Barroca Grande, Portugal

(4) Institute of Earth Sciences (ICT), Pole of University of Porto, Rua do Campo Alegre 687, 4169-007 Porto, Portugal

Manuscript submitted to Earth & Planetary Science Letters, the 26th of January 2018

Abstract: Deciphering the behavior of fluid flow at the magmatic-hydrothermal transition is crucial to understand physical processes leading to the formation of intrusion-related ore deposits and hence to predict the localization of mineralized bodies. However, the hydrodynamics (direction and velocity) of the hydrothermal fluid flow related to this transitional stage remains poorly constrained. Here we present a coupled textural and chemical study performed on tourmaline growth bands to constrain fluid flow during the initiation of the hydrothermal system of the W-Sn-(Cu) Panasqueira deposit. This exceptional deposit consists of a dense network of flat wolframite and cassiterite-bearing quartz veins intensely developed above a well-known hidden greisen cupola. The W-Sn mineralization is preceded by a tourmalinization stage occurring as metasomatic halos around veins and as selvages developed along the vein-wall-rocks contacts. Results emphasize the key role of the greisen cupola on fluid focusing and the role of fluid overpressure during the vein opening. Velocity values highlight an efficient transport of metals in veins largely dominated by advective process (10^{-4} to 10^{-3} $m.s^{-1}$), whereas fluid flow in the altered wall-rocks is slow and pervasive (10^{-6} to 10^{-5} $m.s^{-1}$), suggesting that the element transport through the metasedimentary host rock was low and limited to the alteration haloes. LA-ICP-MS analyses of tourmaline growth bands reveal that fluids coming from the cupola are enriched in Na, K, Li, Sr and Sn, thus emphasizing the contribution of magmatic fluids during the vein formation and the metasomatic alteration of the wall-rocks. More generally, this study demonstrates that the apical portions of granite bodies play as emanative centers of mineralized fluids, and highlights the usefulness of mineral growth band analysis in the search for intrusion-related mineralization.

Keywords: magmatic-hydrothermal activity, Panasqueira, tourmaline, growth bands, flow direction, flow velocity

1. Introduction

The formation of hydrothermal ore deposits and the development of alteration halos in rocks involve the transfer of a large amount of fluids through permeable rocks during several episodic pulses integrated over a long period of time (Barnes, 1997; Robb, 2005). To form a high-grade deposit, the flow of metal bearing fluids must be focused in a restricted space and coupled with an efficient precipitation and trapping mechanism. Hence, understanding hydrothermal fluxes constitutes a major issue of metallogeny and requires resolving some fundamental questions related to: (i) the driving force of fluid flow and (ii) the direction and the velocity of fluid flow. The search for answers to these issues involves a combination of approaches including recognition of permeable pathways (Sibson, 1992; Cox 2005), mineralogical and geochemical analysis (Cartwright and Buick, 1996; Ferry et *al*., 2002) and fluid hydrodynamics (Ingebristen and Appold, 2012).

Among hydrothermal ore deposits, those triggered and driven by magmatic felsic intrusions represent a main primary source of economically important metals, including copper (Cu), tungsten (W), tin (Sn), molybdenum (Mo) and gold (Au) (Hedenquist and Lowenstern, 1994; Černý et *al*., 2005). There is general agreement that these magmatic-related deposits are partly formed by releasing and expulsion of metal-bearing fluids during the emplacement and the cooling of magmatic intrusions (Hedenquist and Lowenstern, 1994; Černý et *al*., 2005). Another important process for metal transport in magmatic-hydrothermal systems is the development of large convective cells around plutons driven by the thermal contrast between intrusive bodies and the host rocks. This convective fluid flow is able to mobilize a large amount of fluids from the surrounding host rock and has a marked effect on the fluid flow patterns (Norton and Cathles, 1979; Eldursi et *al*., 2009). More specifically, it has been commonly observed that mineralized systems are usually centred on small plutons, apices or feeder zones (Dines, 1956; Dilles and Proffett, 1995; Gloaguen et *al*., 2014) suggesting a strong control of the pluton roof geometry on mineralizing fluid flow. Indeed, some numerical models have demonstrated that fluid flow is optimal above the apical part of intrusions and predict the formation of ore deposits in these areas

(Sams and Thomas-Betts, 1988; Eldursi et *al*. 2009; Weis et *al*. 2015). Despite these elegant numerical results, this expected fluid flow pattern (flow direction and velocity) needs to be verified by field investigations.

Moreover, it is widely recognized that magmatic-hydrothermal systems integrate a complex history encompassing episodic stages of fluid flow related to polyphase intrusion emplacement, which have important effects on the geometry of hydrothermal systems. In this scheme, the magmatic-hydrothermal transition is a key event that marks the initiation of the hydrothermal system and defines the future behavior of fluid flow. Indeed, it is usually during this transitional stage that permeable structures open and drain mineralized fluids. However, fluid flow related to this specific hydrothermal stage is difficult to access and thus remains poorly constrained due to the lack of recognized methods to implement in the field.

The textural analysis of mineral growth bands has provided significant information about the direction and velocity of fluid flow involved in the formation of hydrothermal ore deposits (Kessler et *al*. 1972) and during metasomatic processes (Sizaret et *al*., 2009; Majhoubi et *al*., 2016). This direct approach constitutes a powerful tool to constrain fluid flow related to a specific hydrothermal event such as the magmatic-hydrothermal transition. In the present study, we perform a textural analysis of tourmaline growth bands to decipher fluid flow at the initiation of the magmatic-hydrothermal stage of Panasqueira (Portugal). This textural analysis is combined with trace elements analysis of tourmaline growth bands to constrain the chemical characteristics of fluids from which the tourmalines have crystallized. Panasqueira is an historic world-class W vein deposit characterized by a well-preserved magmatic-hydrothermal plumbing system. This deposit is one of the best-documented and characterized in the world and represents a reference site to study magmatic-hydrothermal processes leading to the formation of a Sn-W ore deposit (Thadeu, 1951; Kelly and Rye 1979; Poyla, 1989; Poyla et *al*., 2000; Foxford et *al*., 2000; Lecumberri-Sanchez et *al*., 2017; Codeço et *al*., 2017). From the results of estimated fluid directions and velocities, we discuss the key parameters controlling the behavior of fluid flow at different scales, such as: (i) the role of granitic cupolas on the localization of mineralized areas by fluid flow focusing, (ii) the role of fluid overpressure conditions on vein opening and propagation

of alteration halos in wall-rocks, and (iii) the required duration of fluid flow during the W-Sn mineralization stage.

2. Geological and metallogenic framework

2.1 Regional geology

The W-Sn-(Cu) Panasqueira ore deposit is located in the Central Iberian Zone (CIZ), which constitutes the axial zone of the Iberian Variscan belt (Fig. 1a) (Julivert et *al*., 1972). The CIZ is composed of the Schist-Greywacke-Complex (SGC) intruded by a large volume of granitoid intrusions resulting from an extensive magmatic event during the latest stages of the Variscan orogeny (Dias et *al.,* 1998). The SGC consists of a thick (8-11 km) sequence of late Neoproterozoic schists and greywackes affected by a regional greenschist metamorphism (Martínez-Catalán et *al*., 2007). Deformation of the SGC consists of tight and upright folds with NW-SE sub-vertical axial planes produced by a NE-SW shortening related to the earliest compressive stage of the Variscan orogeny (Dias and Ribeiro, 1995 and Martínez-Catalán et *al*., 2007). This folding is associated with a regional sub-vertical penetrative axial planar cleavage (S1) (Fig. 1a and 1b). The CIZ host numerous Sn-W ore deposits and occurrences related to granitic intrusions and formed by magmatic-hydrothermal processes (Derré, 1982).

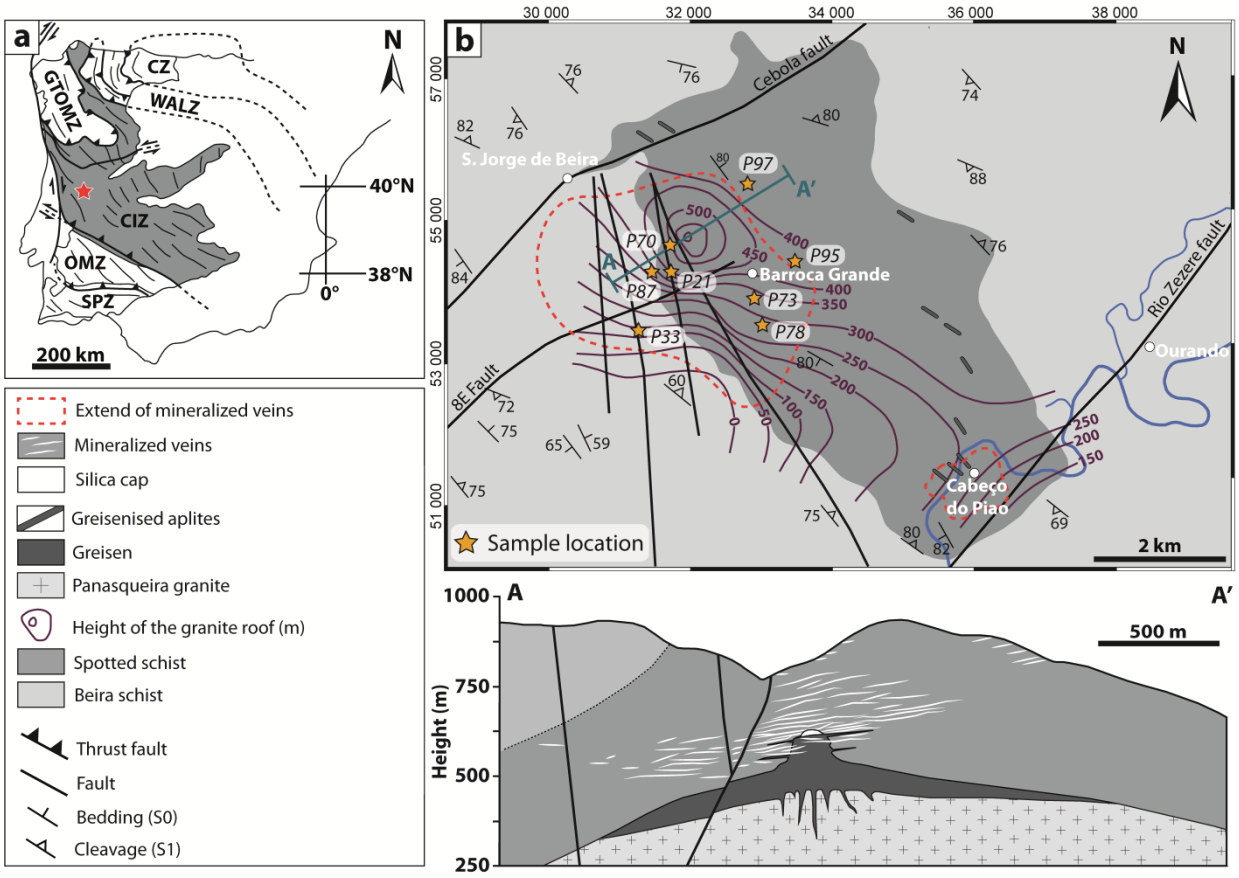


Figure 1 (a) Tectonic map of the Variscan Iberian massif showing the main tectonostratigraphic domains defined by Julivert et *al.*, (1972). The location of the Panasqueira deposit is marked by a red star. CZ: Cantabrian Zone, WALZ: West Asturian-Leonese Zone, GTOMZ: Galicia Tràs-os-Montes Zone, CIZ: Central Iberian Zone, OMZ: Ossa-Morena Zone and SPZ: South Portuguese Zone (b) Geological map of the Panasqueira ore deposit including the height of the granite roof. The (A-A') geological cross section displaying the spatial relationship between mineralized veins and the greisen cupola (data source Beralt Tin & Wolfram S.A.).

138

139 *2.2 The W-Sn-(Cu) Panasqueira ore deposit*

140 The Panasqueira ore deposit is located in the Beira Baixa province in the southern flank of the
141 Serra da Estrela massif constituted by late to post tectonic granitic intrusions. In this region the
142 late Neoproterozoic folded and metamorphosed SGC is locally named Beira Schist. At
143 Panasqueira, spotted schists mark the presence of a thermal metamorphic aureole related to an
144 underlying S-type granite (Thadeu, 1951; Clark, 1964). The intrusive body is limited by the
145 Cebola fault to the north and the Rio Zêzere fault to the south (Fig. 1b) (Clark, 1964). As exposed
146 by underground mining works and drill cores, the upper part of this granite includes a quartz-

147 muscovite greisen cupola formed by interaction between granitic rocks and acidic F-B and Li-rich
148 fluids (Shcherba, 1970; Bishop, 1989) (Fig. 1b and 2a).

149 The W-Sn mineralization is hosted by a dense network of low dipping veins crosscutting the
150 vertical foliation of the Beira Schist and the greisen cupola (Fig. 2a). The veins system is centered
151 above the greisen cupola and extends over an area of 6 km² for a depth extension of about 200-300
152 meters (Fig. 1b) (Kelly and Rye 1979; Poyla et *al*., 2000). This unusual shallow dipping
153 orientation of mineralized veins is compatible with the regional stress field that involved NE-SW
154 shortening with a vertical σ_3 leading to the formation of tight and upright folds accompanied by
155 the development of the regional NW-SE sub-vertical foliation (Dias and Ribeiro, 1995; Martínez-
156 Catalán et *al*., 2007). Based on textural and structural analysis of the vein swarms, Foxford et *al*.,
157 (2000) proposed a crack-and-seal model involving episodic vein dilation and filling induced by
158 injections of fluids at supralithostatic pressure conditions in a compressive crustal regime.
159 Although this mechanism is quite appealing, these conditions of fluid overpressure in veins remain
160 unproven. The structural control of the vein formation has probably induced permeability
161 anisotropy with a strong horizontal component which could affect the pattern of fluid flow at the
162 mineralization time. A late NNW-SSE and ENE-WSW sub-vertical fault system crosscuts the
163 veins and the granite intrusion (Fig. 1b) (Thadeu 1951, Kelly and Rye 1979, Foxford et *al*., 2000).
164 As evidence in the field, these faults postdate mineralization event and have not controlled fluid
165 flow during the W-(Sn) mineralization (Thadeu, 1951).

166 The complex paragenetic sequence of veins was described in detail by Kelly and Rye (1979)
167 and improved by Poyla et *al*., (2000). At least five mineralization stages occurred in the veins
168 from oldest to youngest: the Quartz-Tourmaline (QTS) stage, the Main Oxide Silicate Stage
169 (MOSS), the Main Sulfide Stage (MSS), the Pyrrhotite Alteration Stage (PAS) and the Late
170 Carbonate Stage (LCS). The MOSS (Fig. 2b) and the MSS (Fig. 2c) are the most economically
171 relevant ore stages. The MOSS carries the W-Sn mineralization and consists in muscovite and
172 quartz accompanied by wolframite and cassiterite. The two earliest mineralization stages (QTS
173 and the MOSS) constitute a continuous sequence which is then superimposed and/or cross-cut by
174 the late sulfide stage (MSS). The MSS, which carries the Cu mineralization, is mainly composed

of arsenopyrite, chalcopyrite, sphalerite pyrite and pyrrhotite (Thadeu 1951, Kelly and Rye 1979, Poyla et *al*. 2000). Based on fluid inclusions analyses, Kelly and Rye (1979) and Bussink (1984) have reported that fluids related to the MOSS and the QTS have been trapped at temperatures between 300 and 350°C. Although the tourmaline stage (QTS) is volumetrically of minor importance (mm to cm of thickness), it marks the initiation of the Panasqueira hydrothermal system (Poyla et *al*., 2000).

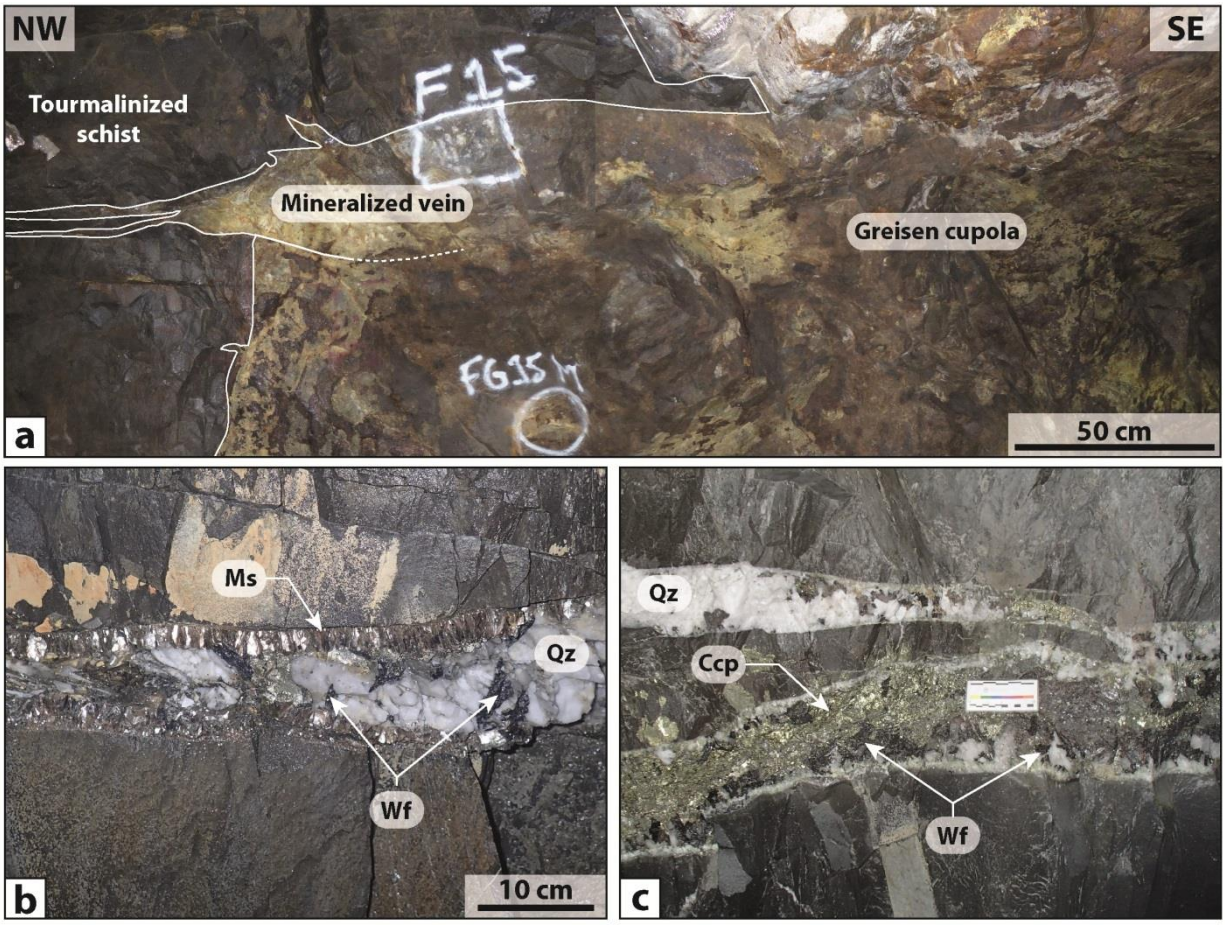


Figure 2 The mineralized system of the W-Sn-(Cu) Panasqueira deposit. (a) Contact between the greisen cupola and the tourmalinized metasedimentary host rock at the level 1 of the mine. Note the presence of mineralized veins which crosscut this contact. (b) Typical Quartz-Wolframite veins corresponding to the main oxide stage. (c) Quartz-Wolframite veins superimposed by the late sulfide stage carrying the Cu mineralization. Abbreviation from Whitney and Evans (2010) Ccp: Chalcopyrite, Ms: Muscovite, Qz: Quartz and Wf: Wolframite.

3. Tourmaline occurrence

At Panasqueira, tourmaline is common, especially in metasedimentary host rock surrounding mineralized veins (Fig. 3a). Tourmaline is present within alteration halos, which are developed along schist-vein contacts within the lower and the upper wall-rocks. These halos result from metasomatic reactions induced by fluid–rock interactions during hydrothermal fluid flow in the veins. Locally, it is possible to observe alternation of quartz-rich and tourmaline-muscovite rich layers inherited from lithological heterogeneities of the Beira Schist. These tourmalines are fine and their trigonal axes are randomly oriented in the vertical cleavage planes of the schist.

Tourmaline is also present in veins along schist-vein contacts (Fig. 3b and 3c). They occur as fine acicular crystals (1-3 mm) with <c> axes vertical and perpendicular to the vein edge and consequently to the inferred plane of fluid flow (Fig. 3c). These tourmalines grains are commonly associated with apatite, rutile and muscovite (Fig. 3d), while their relation with the ore minerals (wolframite and cassiterite) is difficult to observe. However, in some veins tourmaline appears to shortly predate wolframite and can be texturally associated with cassiterite (Fig. 3e). Consequently, tourmaline represents a good candidate to track W-Sn mineralized fluid flow related to the QTS and the MOSS in the Panasqueira veins system.

For both types of tourmaline, the sections normal to the <c> axis are characterized by growth band zonation with a core and well-defined rims (Fig. 3d and Fig. 3f). These bands emphasize an anisotropic growth and highlight a symmetry breakdown due to a directional fluid flow (Fig. 4a and 4b).

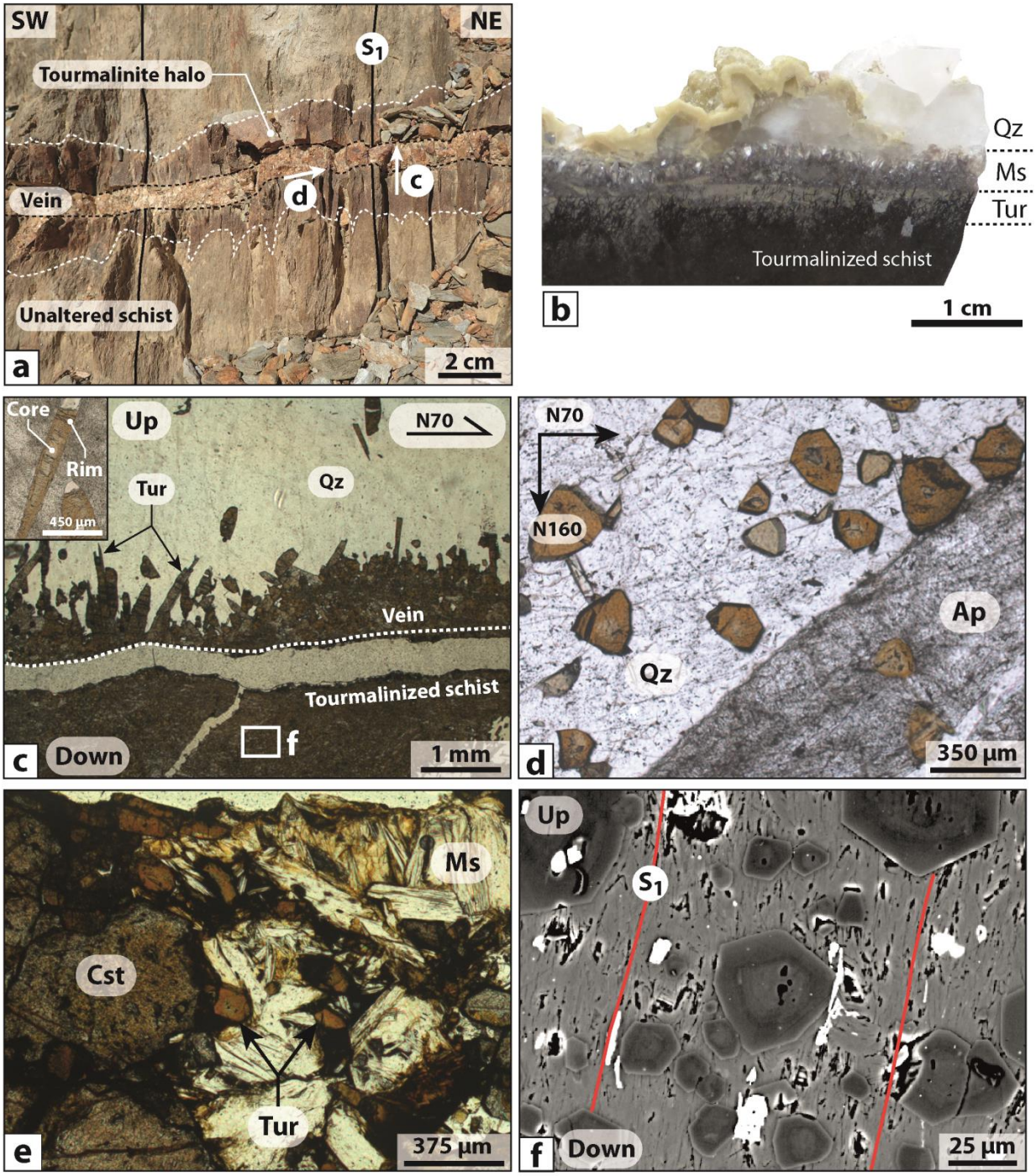


Figure 3 Textural and petrographic characteristics of tourmalines present in the mineralized system of Panasqueira. (a) Quartz-tourmaline vein with tourmalinization of the metasedimentary wall-rocks. The white dashed line indicates the tourmalinization front in the metasedimentary host rock. c and d arrows give orientation of the thin sections c and d. Note the preferential migration of tourmalinization front in the vertical foliation planes S_1 (b) Sample of mineralized veins showing the vertical growth of acicular tourmalines along the schist-vein contact. (c) and (d) photomicrographs of vein tourmaline showing sections parallel (c) and normal (d) to the trigonal axis of tourmaline. (e) Photomicrograph of mineralized vein showing tourmaline grains associated with cassiterite. (f) SEM photomicrograph of altered schist perpendicular to the foliations planes showing growth band zoning in tourmaline basal sections. Abbreviation from Whitney and Evans (2010) Ap: Apatite, Cst: Cassiterite, Ms: Muscovite and Qz: Quartz.

4. Sampling and methodology

Owing to its remarkable mechanical and chemical stability, tourmaline is able to record significant information about its host environment (Henry and Dutrow, 1996; Van Hinsberg et *al*. 2011a). In particular, tourmaline provides a powerful tool to constrain hydrodynamics (direction and velocity of fluid flow) of geological processes involving fluid flow (Sizaret et *al*., 2009; Mahjoubi et *al*., 2015). Moreover, tourmaline incorporates a diversity of traces elements and constitutes a geochemical monitor of fluid compositions (Marks et al., 2013; Van Hinsberg et *al*., 2017). In this study, tourmaline growth bands were used to track both flow and chemical composition of hydrothermal fluids involved during the earliest stages of the vein formation at Panasqueira.

Oriented vein samples with tourmaline were collected in the mine and at the surface, at different places around the cupola, both horizontally and vertically to have a full spatial distribution, and to establish a paleo-fluid flow map around the granitic intrusion (Fig. 1b). Unfortunately, no samples were available in northwestern part of the studied area.

The vertical migration of the alteration front (tourmalinization) within the metasedimentary host rocks appears to be driven by the sub-vertical foliation planes (S1). To study the vertical fluid flow related to the alteration of the wall-rocks, samples of alteration halos have been collected above and below veins perpendicularly to the vertical foliation planes (NE-SW section). The orthogonal NW-SE sections are parallel to the foliation planes and hence do not permit to perform fluid flow reconstruction in the wall rock due to the preferential crystallization of tourmaline in parallel within the foliation planes.

4.1 Fluid flow reconstruction by growth band measurements

In hydrothermal systems, the crystal shape is controlled by its intrinsic symmetry and the effects of external forces, such as fluid flow, that induce anisotropic growth (Curie 1908). The method used for reconstruction of local fluxes is based on the notion that crystal faces exposed to the chemical flux (i.e. the upstream faces) grow faster than downstream faces (Kessler et *al*. 1972 and Sizaret et *al*., 2006 and 2009). The relationship between flow velocity and the relative growth

rate of upstream and downstream faces can be modelled and quantified (Sizaret et *al*. 2006 and 2009). From this postulate, it is possible to deduce local fluid flow directions and velocities in the hydrothermal system. Oriented thin sections were cut parallel to the expected stream-line, i.e. parallel to veins, within the vein, and vertically and perpendicular to foliation planes in altered host rocks. Tourmaline crystals were examined on polished thin sections using optical transmitted light and scanning electron microscope. Then, on tourmaline basal section (i.e., perpendicular to the trigonal axis) the growth band thickness of equivalent crystal faces (d_1, d_2 and d_3) and their respective directions (α_1, α_2 and α_3) have been measured (Fig. 4c). The three normalized thicknesses d_{max}, d_{int} (intermediate) and d_{min} were determined. Assuming that the thickest band (d_{max}) received the largest chemical flux, the orientation of d_{max} gives the direction of the paleo-fluid flow recorded by the crystal (Fig. 4c).

The relationship between fluid velocity and growth ratios (d_{max}/d_{min}) was established by solving the coupled Navier-Stokes and chemical transport equations with the Comsol Multiphysics finite element code (Sizaret et *al*., 2009). In this modeling the edge size of tourmaline is 50 µm and the fluid (water) viscosity is chosen at realistic mineralizing conditions, taken here at 350°C ($7.3.10^{-5}$ Pa.s source NIST WebBook, 2017). Varying flow velocity provides a relationship between chemical flux ratio (upstream/downstream) and fluid velocity (Fig. 4d). The growth band thicknesses measured on minerals can be considered as chemical fluxes integrated over a given period of time. Consequently, the fluid velocity can be determined by inverse method by reporting the measured d_{max}/d_{min} ratio on the flux ratio (Upstream/downstream) vs velocity curve (Fig. 4d) (Sizaret et *al*. 2006 and 2009).

To obtain representative measurements, basal sections of tourmaline were chosen from the following criteria: absence of contact with another crystal of tourmaline, absence of recrystallization and corrosion and easily identifiable equivalent faces.
For each site, flow directions and velocities deduced from each tourmaline section were implemented and treated with the free meteorological software WRPLOT View™ (Lake Environmental, 2016) in order to establish "wind roses" of local paleo-fluid flow. These rose diagrams are then reported on the map.

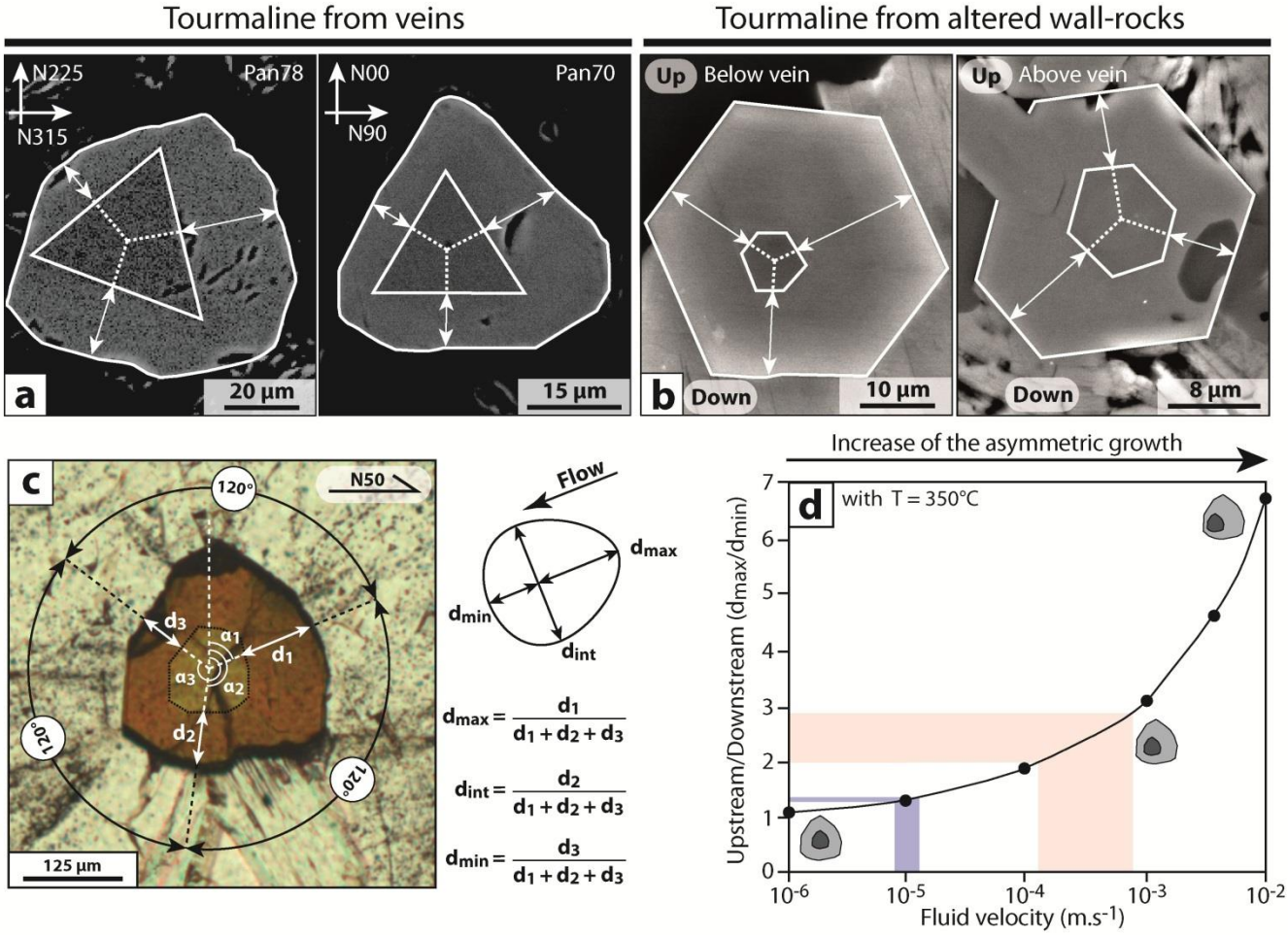


Figure 4 Examples of basal sections of tourmaline from veins (a) and altered wall-rocks (b) displaying an asymmetric shape due to an anisotropic growth (c) Measurements of growth bands thickness and orientation on a basal section of tourmaline. (d) Curve deduced from numerical modeling showing relationship between fluid velocity and flux ratio (see text for details). The filled boxes indicate range of averages of fluid velocities derived from d_{max}/d_{min} ratio measured on tourmalines from altered wall-rocks (blue) and veins (red).

4.2 Tourmaline growth band chemistry

4.2.1 Major and minor element analysis

The major and minor element compositions of tourmaline were determined on polished thin sections using a Cameca SX-Five electron probe micro-analyzers (EPMA) at the Institut des Sciences de la Terre d'Orléans (ISTO). Analyses were performed using an accelerating voltage of 15 kV, a beam current of 6 nA with a diameter of 2 µm. The elements analyzed were Si, Ti, Al, Fe, Mn, Mg, Ca, Na, K, F and Cl. For calculation of the structural formulae and site allocation in tourmaline, analyses were normalized to 15 cations (T + Z + Y-sites) and B_2O_3 and H_2O contents

were calculated by stoichiometry, considering B = 3 apfu and OH + F + Cl = 4 apfu. Analytical conditions and calibration are detailed in electronic supplementary materials (ESM1).

4.2.2 Trace element analysis

Trace element concentrations in tourmaline were determined by laser ablation inductively coupled plasma-mass-spectrometry (LA-ICP-MS). These analyses were performed at BRGM (French Geological Survey) using a ThermoScientific X series II quadrupole ICP-MS coupled with a Cetac Excite 193 nm laser ablation system. Ablations were performed with a repetition rate of 8Hz and laser energy of 3.5 J/cm² with a beam size of 40 µm. Analyses comprise 20 seconds of gas blank measurement following by 60 seconds of ablation. Elements analyzed were ^{7}Li, ^{23}Na, ^{24}Mg, ^{27}Al, ^{29}Si, ^{47}Ti, ^{51}V, ^{55}Mn, ^{66}Zn, ^{88}Sr and ^{118}Sn. Data reduction was performed with the software Glitter 4.0 using the NIST SRM-612 glass standard for external standardization and ^{29}Si as the internal standard. Concentrations in Mg and Al obtained by LA-ICP-MS data reduction were compared with EPMA analyses to check the accuracy of the results. Analyses of certified standard NIST-612 SRM give a good accuracy with a relative standard deviation (RSD) below 10%. Detection limits for most elements range between 0.2 and 5 ppm. Higher detection limits were achieved for Zn, Ti and Na (respectively 5.5 ppm, 15.4 ppm and 37.4 ppm).

5. Results

5.1 Large scale fluid flow

Fluid flow directions and velocities are summarized in Table 1 (complete measurements in electronic supplementary materials ESM2) and illustrated in Figure 5. For veins-hosted tourmaline, an average ratio of d_{max}/d_{min} was determined for each of the 8 sample sites. These average ratios range from 2.0 to 2.9 implying a fluid velocity varying from 10^{-4} to 10^{-3} m.s^{-1} in veins (Table 1 and Fig. 4d). Figure 5c shows the histogram representation of all velocity values, which are characterized by an asymmetric distribution centered on 10^{-4} - 5.10^{-4} m.s^{-1}. This wide variable distribution is probably due to the sinuous nature of the fluid flow path. Indeed, a narrowing of the pathway can be responsible of the local high velocity value recorded by some tourmalines. For each sample of veins, the flow directions are dispersed with a significant mean

direction (Fig. 5a). In the "rose" diagrams, these directions generally host the highest velocity values (10^{-4} to 10^{-3} m.s^{-1}). Conversely, lowest fluid velocity values are not aligned with these mean directions of fluid flow (Fig. 5a). Considering all the sites, the mean orientations of flow depict a large-scale streamline structure with radial directions coming from a center located on the greisen cupola (Fig. 5a and 5b). The vertical fault system crosscutting the veins does not influence flow direction in the veins (Fig. 5b). The pitch of flow direction vectors on the vein plane is not aligned to the dip direction of veins (Table 1). Consequently, flow directions are not influenced by veins orientation.

5.2 Fluid flow in host rock

In altered schist, tourmaline growth bands show a fluid flow escaping sub-vertically from veins toward the host rock, with an averaged angle of 55° above and 60° below the vein (Fig. 6). This symmetrical behavior may be related to the horizontal component of fluid flow within the vein, as suggested by measurements on the P21 sample. Mean velocities obtained in altered wall-rocks are 1 to 2 orders of magnitude lower than fluid velocity obtained in the veins (Fig. 4d and Fig. 6). In addition, it would appear that velocities are higher above (10^{-5}- 5.10^{-5} m.s^{-1}) than below veins (5.10^{-6} to 10^{-5} m.s^{-1}) (Fig. 6).

	Coordinates (ETR S89/Portugal TM06)			Veins orientation		d_{max}/d_{min}			Fluid flow		
Veins:	X (m)	Y (m)	Z (m)	Strike	Dip	N	Mean	SD	Mean direction	Mean velocity ($m.s^{-1}$)	Pitch
Pan70	31675.9	54649.3	620	N136	7°	30	2.06	0.66	N28	2.76E-04	77°
Pan87	31410.9	54261.6	620	N300	5°	41	2.50	0.95	N64	6.65E-04	60°
Pan21	31675.1	54253	560	N200	5°	31	2.06	1.06	N27	5.53E-04	10°
Pan33	31217.9	53385.2	470	N130	15°	24	2.24	0.39	N40	3.33E-04	90°
Pan78	33043.4	53490.3	618	N138	7°	31	2.29	1.13	N331	6.66E-04	26°
Pan73	32933.2	53875.3	662	N127	10°	25	2.75	1.10	N321	9.46E-04	24°
Pan95	33058.4	54287	741	N127	5°	18	2.92	1.27	N300	1.38E-03	8°
Pan97	32833.3	55559.5	732	N160	10°	25	2.74	0.96	N201	9.47E-04	42°
Altered wall-rocks :											
P20 Up	31675.1	54253	560	-	-	28	1.36	0.18	55	1.44E-05	-
P20 Down	31675.1	54253	560	-	-	28	1.29	0.11	60	6.95E-06	-

Table 1 Results of directions and velocities of fluid flow deduced from tourmalines growth bands in veins and in altered wall-rocks (SD: Standard Deviation and N: number of measurement).

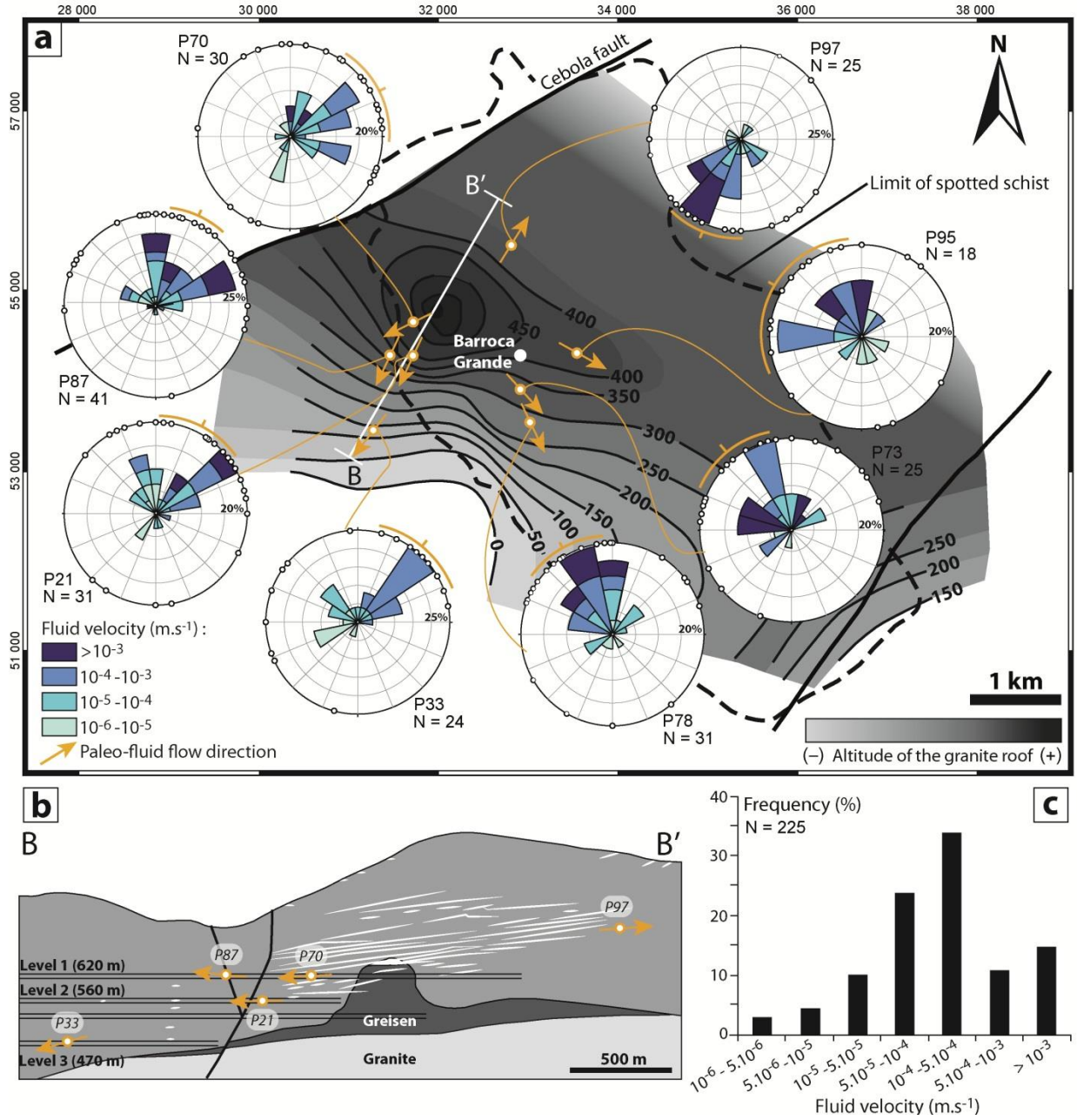


Figure 5 Results of fluid flow at the ore deposit scale deduced from tourmaline growth bands in mineralized veins. (a) Large scale map of paleo-fluid flow around the hidden granite of Panasqueira. Local fluid flow direction and velocities are represented with "rose" diagrams, which give direction of tourmaline faces exposed to the fluid flow (d_{max}) and directional distr<ibution of fluid velocities. The orange arcs give the 95% interval of confidence, from where the fluid comes. The orange arrows on the map correspond to the mean directions of flow determined for each sample site. N corresponds to the number of measurements performed for each sample sites. (b) Results of fluid flow projected on the geological cross section (B-B') showing flow moving away from the cupola. (c) Histogram showing distribution of all fluid velocity values.

332

333

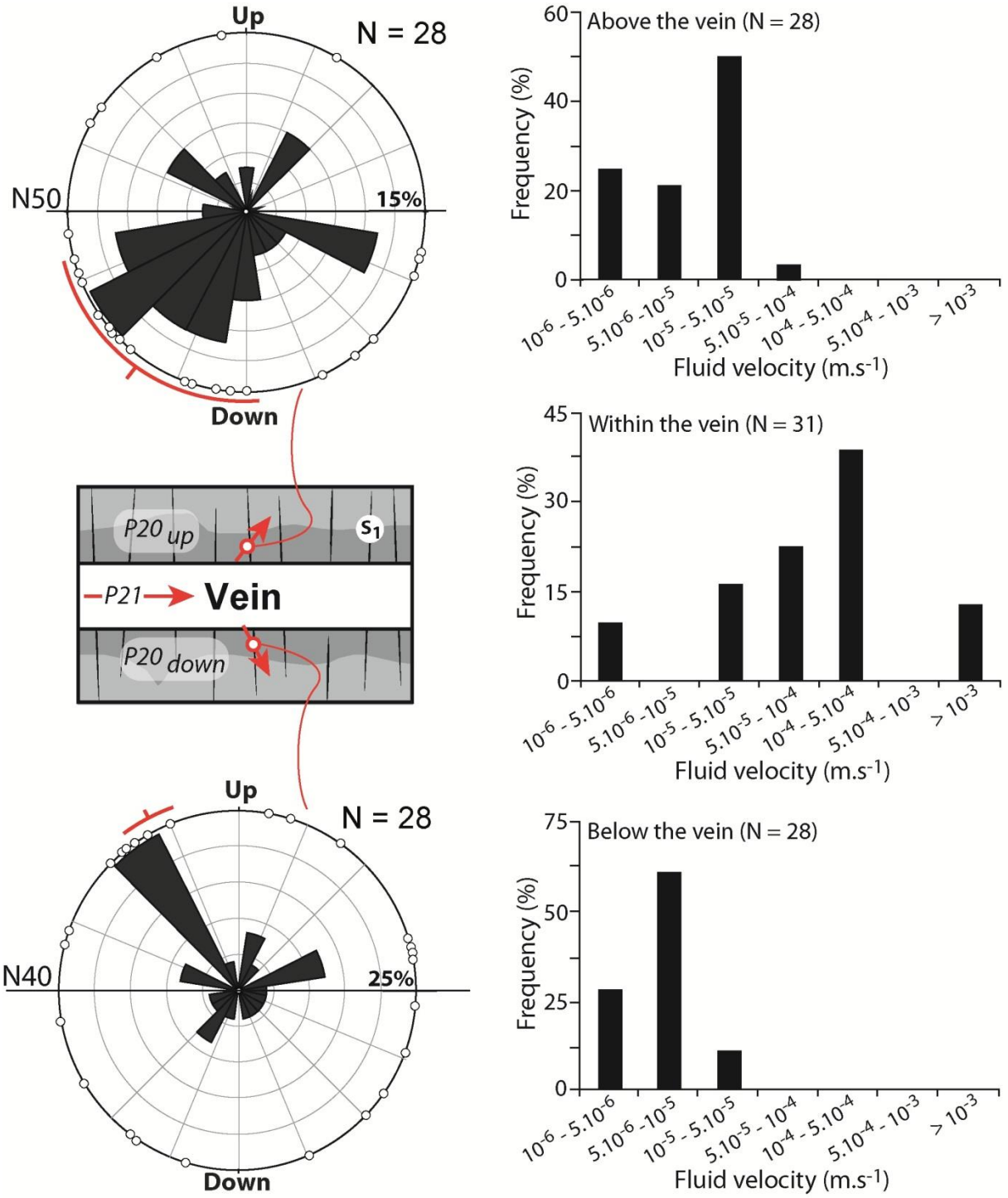


Figure 6 Sketch showing vertical paleo-fluid flow deduced from tourmaline in altered wall-rocks. Fluid flow directions are represented with rose diagrams giving direction of faces exposed to fluid flow. The red arcs indicate the 95% interval of confidence, from where the fluid comes. Velocity values obtained above, below and within the vein are presented in histogram diagrams. N corresponds to the number of measurement performed for each sample.

334

335

336

337 *5.3 Tourmaline growth band compositions*

338 Chemical compositions of tourmalines are summarized in Table 2 (complete analyses in
339 electronic supplementary materials ESM3 and ESM4). General features and classification of
340 Panasqueira tourmalines have already been described by Codeço et *al*., (2017). Here, we focus on
341 compositional differences in minor and trace elements between core and growth band used for
342 fluid flow reconstruction. It appears that this growth band zoning is systematically associated with
343 chemical variations in major, minor and trace elements (Table 2). In the veins, cores and rims of
344 tourmaline exhibit compositions that suggest equilibration with Li-depleted granitic rocks (Fig.
345 7a). However, rims are richer in Fe and poorer in Mg and Al than cores. In altered wall-rocks,
346 cores are characterized by a wide range of compositions suggesting equilibration with
347 metasedimentary host rocks and Li-depleted granitic rocks; whereas rims exhibit a more restricted
348 composition identical to rims of veins-tourmalines and that suggest equilibration with Li-depleted
349 granitic rocks (Fig. 7a). This range of core compositions (in altered wall-rocks) reflects the
350 contribution of hydrothermal fluids and the metasedimentary host rocks during the core
351 crystallization of tourmaline.

352 It is generally accepted that magmatic fluids contain significant amounts of Na, K and Cl. As a
353 result, the trace el~~e~~ement concentrations in cores and rims of tourmaline ~~contents of core and rims~~
354 ~~of tourmaline~~ are plotted as a function of the Na concentration to show the possible evolution of
355 the magmatic contribution during tourmaline crystallization. Cores of tourmalines from veins and
356 from altered wall-rocks are characterized by the same compositional ranges. This observation is
357 also valid for rims (Table 2 and Fig. 7b). Consequently, crystallization of tourmalines in the veins
358 is probably contemporaneous with the development of tourmalines in the altered wall-rocks. In
359 addition, results show strong compositional differences between core and rims of tourmalines (Fig.
360 7b). Indeed, the core to rim enrichment in Na is positively correlated with core to rim enrichments
361 in K, Ti, Li, Mn, Sn, and Sr (Fig. 7b). Average concentrations in rims display high contents of Li,
362 K, Mn, Ti and Zn (several hundreds to thousands of ppm) and moderate concentrations of Sn and
363 Sr (several tens of ppm). Conversely, cores are characterized by lower trace element abundances
364 (< 100 ppm for most elements).

These compositional differences between cores and rims, which are similar in the veins and in the wall-rocks, suggest that tourmalines were formed during two distinct stages. The first stage is related to core crystallization (both in veins and in wall-rocks) whereas the second stage is related to the rim overgrowths.

The absence of experimental partitioning coefficients between tourmaline and hydrothermal fluids do not permit to quantify the chemical signature of the hydrothermal fluid from which tourmaline has crystallized. Nevertheless, according to Van Hinsberg et *al*., (2011a; 2017), the compositional changes between cores and growth bands provide a robust tool to track external changes in the trace-element budget of fluids from which tourmalines have crystallized. The present study suggests that rims have crystallized from a fluid richer in Na-K-Sn-Li-F-Zn than the fluid from which cores crystallized.

	Tourmaline from veins				Tourmaline from altered wall-rocks			
	Core		Rim		Core		Rim	
wt%	Ave (n= 20)	Stdev	Ave (n= 20)	Stdev	Ave (n = 20)	Stdev	Ave (n = 20)	Stdev
SiO_2	35.74	0.54	35.14	0.53	34.94	1.43	35.34	0.46
TiO_2	0.18	0.04	0.48	0.08	0.19	0.07	0.46	0.08
Al_2O_3	33.79	0.56	31.10	0.82	34.40	1.07	30.18	0.47
FeO	10.86	0.70	14.23	0.59	8.89	0.83	13.29	0.95
MnO	0.05	0.05	0.11	0.08	0.04	0.06	0.08	0.06
MgO	2.60	0.62	1.31	0.36	3.82	0.54	2.62	0.63
CaO	0.04	0.05	0.08	0.04	0.09	0.05	0.03	0.05
Na_2O	1.39	0.10	2.07	0.20	1.69	0.14	2.26	0.13
K_2O	0.02	0.00	0.05	0.01	0.02	0.01	0.06	0.01
F	0.00	0.01	0.00	0.00	0.00	0.00	0.00	0.00
Cl	0.00	0.00	0.01	0.01	0.01	0.01	0.01	0.01
Total	84.68		84.57		84.09		84.34	
ppm	Ave (n= 16)	Stdev	Ave (n= 17)	Stdev	Ave (n= 11)	Stdev	Ave (n= 14)	Stdev
Li	28	9.6	175	82	43	24	211	33
Na	8399	1049	17190	1739	6843	1887	14514	1463
Ti	1146	211	2465	390	2096	660	3318	269
V	84	29	98	27	61	63	55	16
Mn	413	42	698	125	171	63	542	43
Zn	545	80	908	181	302	105	853	78
Sr	14	6.3	40	9.3	29	18	41	5.5
Sn	9.6	2.9	18	6.1	9.1	6.0	14	3.8

Table 2 Summary of EPMA and LA-ICP-MS results for core and rim of tourmaline from veins and altered wall-rocks

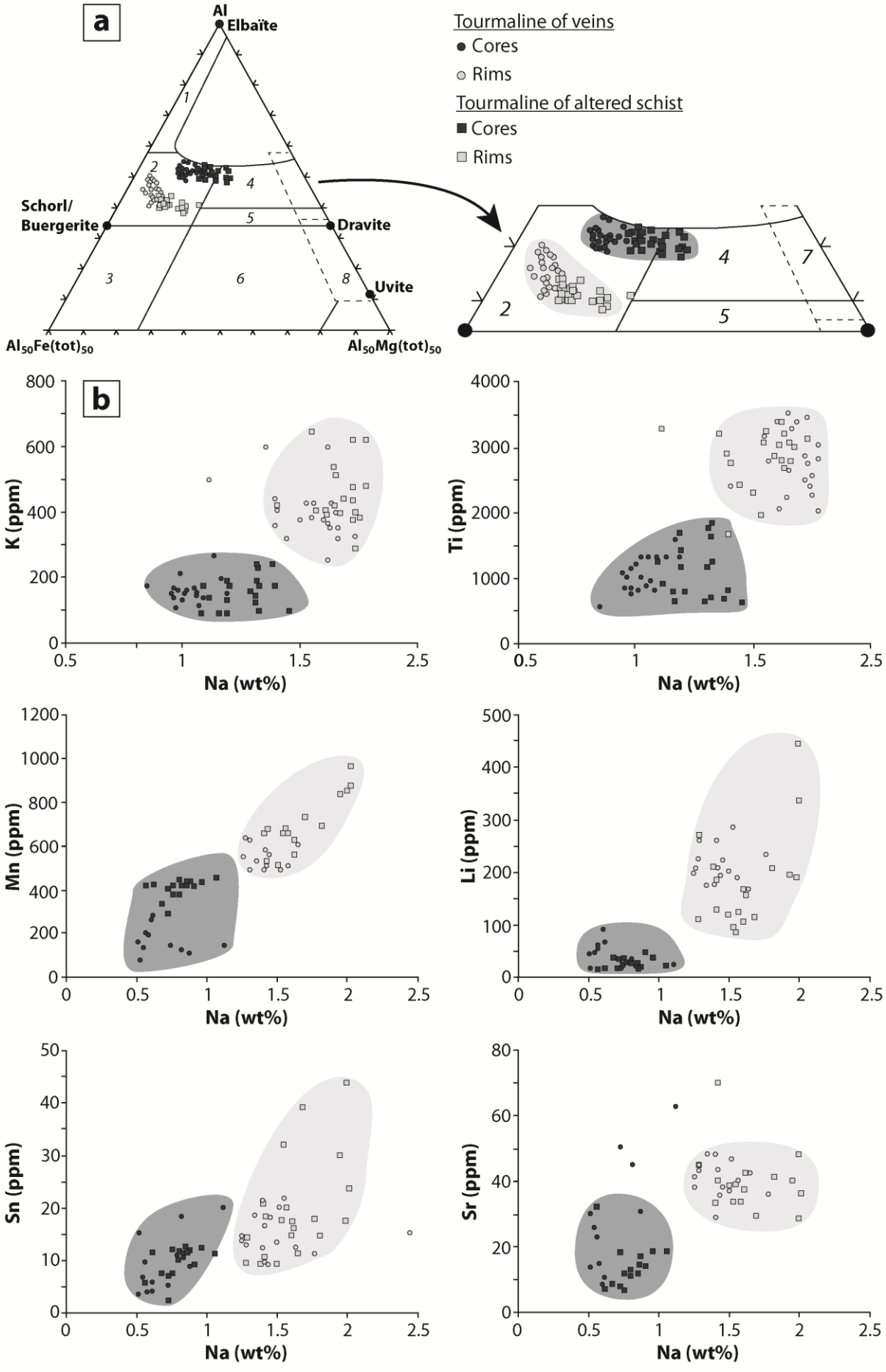

a
Al
Elbaïte
Schorl/
Buergerite
Dravite
Uvite
Al50Fe(tot)50
Al50Mg(tot)50
1
2
3
4
5
6
7
8
Tourmaline of veins
Cores
Rims
Tourmaline of altered schist
Cores
Rims
b
K (ppm)
Ti (ppm)
Mn (ppm)
Li (ppm)
Sn (ppm)
Sr (ppm)
Na (wt%)

Figure 7 Geochemical characteristics of tourmalines used for fluid flow reconstruction in veins and in altered wall-rocks. (a) $Al_{50}Fe_{50}$-$Al_{50}Mg_{50}$ ternary diagram showing relation between tourmaline compositions and crystallization environment (from Henry and Guidotti, 1985). (1) Li-rich granitoids, pegmatites and aplites; (2) Li-depleted granitoids, pegmatites and aplites; (3) Fe^{3+}-rich hydrothermaly altered granitoids; (4) Metapelites and metapsammites with Al-saturating phase; (5) Metapelites and metapsammites without Al-saturating phase; (6) Fe^{3+}-rich metapelites and calc-silicate rocks with quartz and tourmaline; (7) Cr-V-rich metapelites and Ca-depleted meta-ultramafics rock; (8) Meta-carbonates and meta-pyroxenites. (b) Elements variation diagrams showing chemical core-rim evolution of tourmalines in minor (Na, K and Ti) and trace (Li, Mn, Sn and Sr) elements.

6. Discussion

6.1 Role of the granitic cupola on focusing fluid flow

In hydrothermal systems, fluid velocity is proportional to pressure gradient and its average direction is parallel to this gradient. Here, our spatial distribution and orientations of flow velocities suggest a high-pressure zone centered on the greisen cupola with a lateral pressure gradient triggering fluid flow in veins. Hence, hydrothermal fluids have probably been injected into the vein system from the cupola, which, consequently, represents the emanative center from where mineralizing fluids rose and spread laterally in veins. Moreover, the ΣNa/ΣK ratio determined by Poyla et *al*., (1989) for the ore-forming fluids (W-Sn stage) suggests an extensive interaction of these fluids with the underlying granite at 350-400 °C and 1 kbar. The rim compositions of tourmaline confirm an equilibration of fluids with granitic rocks. Furthermore, the extensive greisenisation in the apical part of the granite provides evidence of this equilibration and corroborates our interpretation of a fluid flow focused by the cupola.

This fluid flow pattern can explain the spatial correlation commonly observed between localization of mineralized systems and emplacement of granitic cupolas (Dines, 1956; Dilles and Proffett, 1995). Indeed, it has been proposed that magmatic fluids are preferentially expelled from cupolas, and that can disturb the pattern of convective fluid flow around intrusions by relocating convective cells and discharge zones (Norton and Cathles, 1979; Eldursi et *al*., 2009). Hydrothermal fluxes determined in this study provide direct evidence of the control of apices on focusing of mineralizing fluids. This behavior of fluid flow can be explained by a preferential localization of thermo-mechanical instabilities around apices (Guillou-Frottier and Burov, 2003),

which, when coupled with a preferential accumulation of fluids, leads to opening of permeable structures in which mineralizing fluids are then discharged.

Hence, the apical parts of plutonic intrusions represent convergence spots for hydrothermal fluids and thus are favorable zones for deposition of high grade mineralization. As a result, the approach applied in this study can be useful for mining exploration as pathfinder to discover hidden granitic cupolas and thus locate the emanative centers of mineralizing fluids.

6.2 Fluid escape in wall-rocks and role of fluid on vein opening

The vertical escape of fluids from veins toward metasedimentary host rock involves a vertical pressure gradient with overpressured fluid conditions in veins, causing pervasive fluid flow in the wall-rocks. This interpretation is consistent with the presence of alteration fronts observed around veins (Fig. 3a). Besides, Lecumberri-Sanchez et *al*., (2017) have demonstrated that schists proximal to the veins are systematically enriched in K, B, Sn and W. The rims of tourmalines present in altered wall-rocks are also enriched in certain of these elements (K and Sn). This is consistent with extensive fluid–rock interaction triggered by fluids coming from veins.

According to the rim compositions of vein-and schist-tourmalines, fluid flow in veins can be considered contemporaneous with pervasive fluid flow in altered wall-rocks. As shown above, fluid flow in wall-rocks is related to overpressured conditions in veins. Thus, our results suggest that veins opening and dilation have been induced by injection of fluids at supralithostatic conditions such as proposed by Foxford et *al*., (2000). The low velocity values (not exceeding 5.10^{-5} $m.s^{-1}$) obtained in altered wall-rocks imply a low permeability in the host rocks. As a result, the element transport through the host rock was probably low and limited to the alteration haloes.

Based on the removal of iron (Fe) from the wall-rocks during fluid-rock interactions, Lecumberri-Sanchez et *al*., (2017) suggest that some elements such as Fe have migrated from the host rocks toward veins. At first sight, this chemical flux seems to be incompatible with the direction of fluid flow discussed above. However, iron migration through the host rocks was probably driven by diffusion following a strong chemical gradient between fluid in veins and metasedimentary host rocks, whereas fluid flow was driven by pressure gradient. These two

processes have not involved the same driving force, and it is, therefore, possible to observe a chemical flux that is characterized by a vector that is opposed to the fluid flow direction.

6.3 Velocity analysis and estimation of fluid flow duration during the QTS-MOSS

In this study, the mean fluid flow velocity deduced from veins tourmalines (10^{-4} m.s^{-1}) is high and close to values obtained with the same method in the same type of deposit by Sizaret et *al*., (2009) and Mahjoubi et *al*., (2016), and suggests an efficient metal transport in veins. Considering a porous media with an averaged porosity of 1%, the conversion of this mean velocity to a Darcy velocity (V_{Darcy} = V*porosity) gives a value of 10^{-6} m.s^{-1}. Darcy velocities obtained in contact metamorphic aureoles from mineral reactions and by numerical modeling range respectively from 10^{-9} to 10^{-11} m.s^{-1} (Ferry et *al*., 2002), and from 10^{-8} to 10^{-11} m.s^{-1} (Eldursi et *al*., 2009). It appears that velocities obtained in this study are 2 to 5 order of magnitude higher than those deduced from mineral reactions and numerical modeling. This difference may be due to the fact that velocities obtained from mineral growth bands are valid for a specific hydrothermal stage occurring over a short period of time, while those deduced from other methods are integrated over a larger scale and for the total duration of the hydrothermal system (Ingebritsen and Manning, 1999).

It is widely agreed that the overall time span of hydrothermal activity encompasses multiple fluid pulses, each of them occurring over only a short period of time. If geochronological methods allow dating hydrothermal activity, the uncertainties of these analytical methods do not always permit the estimation of the fluid flow duration for a specific stage. As in most cases, the Panasqueira deposit was formed during a long period of time lasting about 4.2 Myr (Snee et *al*., 1988) but subdivided into several pulses. Here we propose the use of the mean fluid velocity value obtained from veins-tourmaline to estimate the fluid flow duration required for the vein formation during the QTS and MOSS. To do this, we assume that the QTS and the MOSS were formed during the same continuous hydrothermal event with a constant fluid flow velocity. According to Poyla et *al*., (1989) the total volume of fluid that flowed through the vein system during the MOSS is about 1000 km^3 with 0.2 ppm of dissolved WO_3. Considering a total volume of vein about 0.003 to 0.006 km^3 extending over an area of 6 km² (Hebblethwaite and Antao, 1982) characterized by an elliptical shape, we can calculate the surface of the vertical section of fluid flow. From this

surface and the mean fluid flow velocity (10^{-4} m.s^{-1}) we obtain a fluid flow duration ranging from 35 000 to 70 000 years. This is consistent with the short time duration of mineralization emplacement estimated for a single magmatic-hydrothermal event (spanning only about 10 000 to 200 000 years) from numerical modeling (Cathles et *al*., 1997; Chelle-Michou et *al*., 2017) and radiometric dating (Parnell, 1998).

6.4 Hydrodynamic model of the Panasqueira deposit

Our results must be considered as 'snapshot' of the fluid flow at the incipient phase of the hydrothermal system of Panasqueira, corresponding to the magmatic-hydrothermal transition. Considering chemical characteristics of tourmalines and our fluid flow reconstruction, a hydrodynamic model subdivided into two stages is proposed for the early hydrothermal event preceding the main stage of W-Sn mineralization (Fig. 8). The first stage is related to the core crystallization of tourmalines and involves an initial flow of boron-rich fluids. These fluids are partly buffered by the metasedimentary host rocks for Al, Mg and Fe during the crystallization of tourmaline in the wall-rocks (Fig. 7a). This first pulse does not seem to be associated with any W-Sn mineralization. This is consistent with the low contents in trace elements in cores of tourmaline. We have no information about directions of fluid flow related to this first pulse. However, the chemical equilibration of cores of veins-tourmalines with Li-depleted granitic rocks suggests that the first stage can be related to a first expulsion of magmatic fluid during granite crystallization.

The second stage is recorded by tourmaline growth bands and is related to the flow of the mineralized (Li-K-Na-Sn)-rich fluid in the veins system. During this second stage, the external convecting fluids and magmatic fluids released by granite crystallization are both focused by the cupola, which causes the greisenization in the apical part of the granite (Fig. 8). This focused fluid flow is injected into the vein system, whose the significant horizontal permeability anisotropy induces a horizontal fluid flow along the vein planes. The low permeability of the metasedimentary host rock promotes fluid pressure increase leading to the vein opening when fluid pressure reaches supralithostatic conditions (Fig. 8). The velocity contrast between veins (10^{-4} to 10^{-3}m.s^{-1}) and altered wall-rocks (10^{-6} to 10^{-5} m.s^{-1}) emphasize this strong contrast of

permeability and suggests that fluid flow was mainly channeled in the vein system. This channelization of mineralizing fluids in veins could contribute to form a high grade deposit by an efficient metal transport in structural trap sites. The overpressured condition in veins enhances fluid-rock interaction and triggers a pervasive fluid migration in the wall-rocks (Fig. 8). According to Lecumberri-Sanchez et *al*., (2017), the metasedimentary host rock is mainly affected by tourmalinization and muscovitization reactions, which are crucial for the wolframite deposition by iron releasing into the fluid. Finally, the escape of fluids toward the wall-rocks observed in this study can constitute a crucial mechanism for the wolframite deposition by promoting fluid-rock interactions.

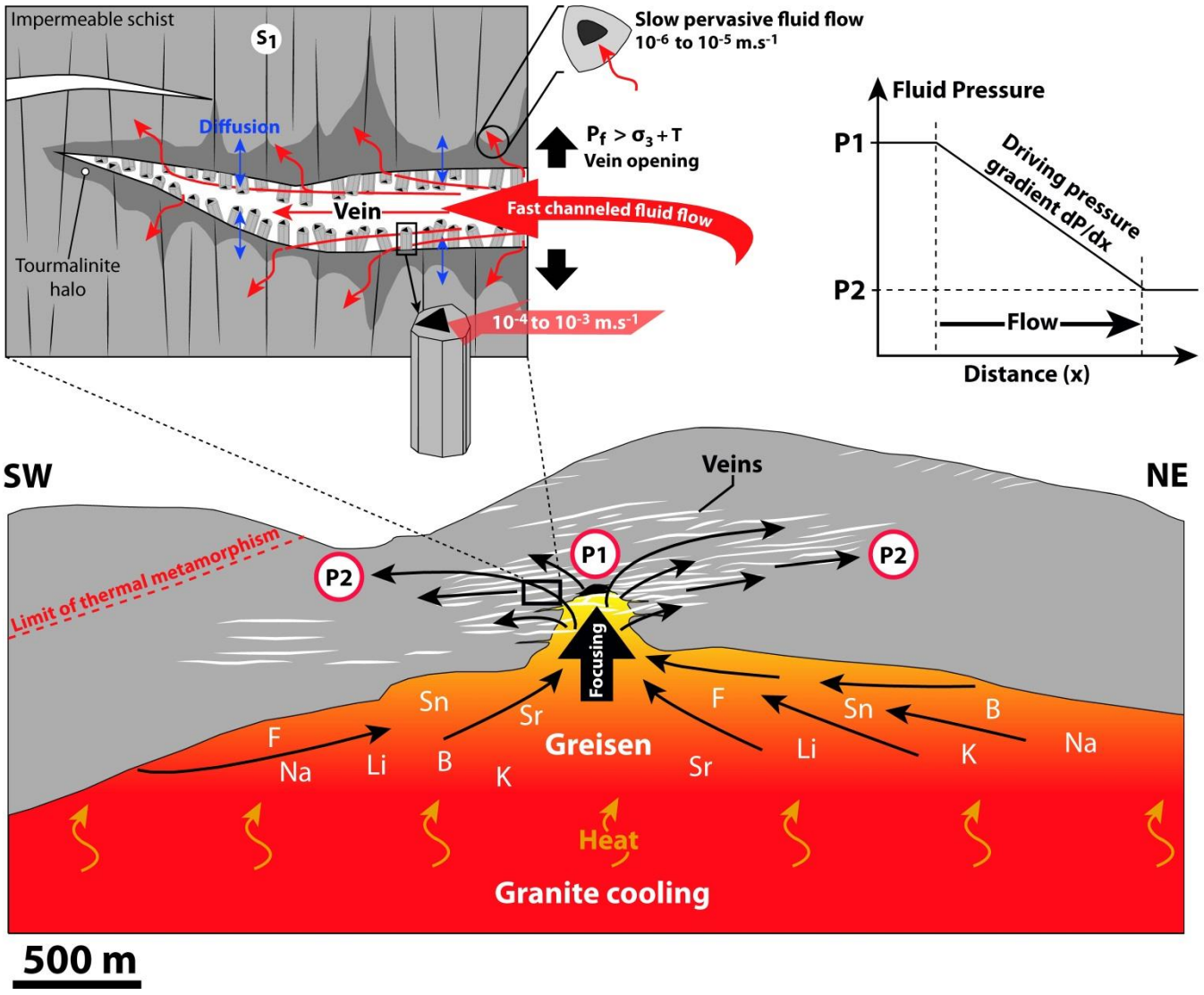


Figure 8 Hydrodynamic model of fluid flow at the magmatic-hydrothermal transition of the W-Sn-(Cu) Panasqueira deposit (drafted on simplified cross section from Thadeu, 1951). With P_f: the fluid pressure condition, σ_3: the vertical stress and T: the tensile strength.

Acknowledgments

We are greatly thankful to Beralt Tin & Wolfram S.A. for the possibility to access to the Panasqueira underground mine. We thank Paolo Ferraz for help during the collection of samples in mine and for discussions about our results. We further would like to thank P. Lach for assistance in LA-ICP-MS analyses and proceeding of data. We are grateful to anonymous reviewers for their constructive remarks, which have greatly improved this manuscript. This research was financially supported by the French Geological Survey (BRGM), Region Centre, the Labex Voltaire (ANR-10-LABX-100-01) and has also taken part of the ERAMIN project "New Ores".

References

Barnes, H.L. 1997. Geochemistry of Hydrothermal Ore Deposits, third ed. John Willey and Sons, New York.

Bishop, A.C. 1989. Greisen. In: Petrology. Encyclopedia of Earth Science. Springer, Boston, MA.

Bussink, R.W. 1984. Geochemistry of the Panasqueira Tungsten-Tin Deposit, Portugal. Geol. Ultraiectina.

Cartwright, I., Buick, I.S. 1996. Determining the direction of contact metamorphic fluid flow: an assessment of mineralogical and stable isotope criteria. J. Metamorph.Geol. 14, 289–305.

Cathles, L.M., Erendi, A.H.J. & Barrie, T. 1997. How long can a hydrothermal system be sustained by a single intrusive event? Econ. Geol., 92: 766-771.

Černý, P., Blevin, P.L., Cuney, M. and London, D. 2005. Granite-Related Ore Deposits. In: J.W. Hedenquist, J.F.H. Thompson, R.J. Goldfarb, and J.R. Richards (eds.). Economic Geology - One Hundredth Anniversary Volume, 337–370.

Chelle-Michou, C., Rottier, B., Caricchi, L. and Simpson, G. 2017. Tempo of magma degassing and the genesis of porphyry copper deposits. Nature Scientific Reports 7, Article number: 40566.

Clark, A. H. 1964. Preliminary study of the temperatures and confining pressures of granite emplacement and mineralization, Panasqueira, Portugal: Inst. Mining MetallurgyTrans., 73, 813-824.

Codeço, M., Weis, P., Trumbull, R., Pinto, F., Lecumberri-Sanchez, P., Wilke, F. 2017. Chemical and boron isotopic composition of hydrothermal tourmaline from the Panasqueira W-Sn-Cu deposit, Portugal. - Chemical Geology (online).

Cox, S.J. 2005. Coupling between Deformation, Fluid Pressures, and Fluid Flow in Ore-Producing Hydrothermal Systems at Depth in the Crust. In: J.W. Hedenquist, J.F.H. Thompson, R.J. Goldfarb, and J.R. Richards (eds.). Economic Geology - One Hundredth Anniversary Volume, 39–75.

Curie P. 1908. Œuvres, 118p. Gautier-Villars, Paris, Société Française de Physique. Reprinted: Archives contemporaines, Paris 1984.

Derré, C. 1982. Caractéristiques de la distribution des gisements à étain-tungstène dans l'ouest de l'Europe. Mineral. Deposita 17:55-77.

Dias, R. & Ribeiro, A. 1995. The Ibero Armorican Arc: a collision effect against an irregular continent? Tectonophysics, 246: 113-128

Dias, G., Leterrier, J., Mendes, A., Simões, P., Bertrand, J.M. 1998. U-Pb zircon and monazite geochronology of syn- to post-tectonic Hercynian granitoids from the central Iberian Zone (northern Portugal). Lithos 45, 349–369.

Dilles, J.H., Profett, J.M. 1995. Metallogenesis of the Yerington batholith, Nevada, in: F.W. Pierce, J.G. Bolm (Eds.), Porphyry Copper Deposits of the American Cordillera, American Geological Society Digest 20, , pp. 306-315.

Dines, H.G. 1956. The metalliferous mining region of South-West England. 2 volumes, HMSO, London.

Eldursi, K., Branquet, Y., Guillou-Frottier, L., Marcoux, E. 2009. Numerical investigation of transient hydrothermal processes around intrusions: Heat-transfer and fluid-circulation controlled mineralization patterns. Earth and Planetary Science Letters 288, 70-83.

Ferry, J., Wing, B., Penniston-Dorland, S., Rumble, D. 2002. The direction of fluid flow during contact metamorphism of siliceous carbonate rocks: new data for the Monzoni and Predazzo aureoles, northern Italy, and a global review. Contrib. Mineral. Petr. 142,679-699.

Foxford, K.A., Nicholson, R., Polya, D.A., Hebblethwaite, R.P.B. 2000. Extensional failure and hydraulic valving at Minas da Panasqueira, Portugal: Evidence from vein spatial distributions, displacements and geometries. J. Struct. Geol. 22, 1065‑1086.

Gloaguen, E., Branquet, Y., Chauvet, A., Bouchot, V., Barbanson, L. and Vigneresse, J.L. 2014. Tracing the Magmatic/Hydrothermal Transition in Regional Low-Strain Zones: The Role of

Magma Dynamics in Strain Localization at Pluton Roof, Implications for Intrusion-Related Gold Deposits. Journal of Structural Geology 58: 108–121.

Guillou-Frottier, L., Burov, E. 2003. The development and fracturing of plutonic apices: implications for porphyry ore deposits. Earth & Planetary Science Letters, 214, 341-356.

Hebblethwaite, R. P. B., and Antao, A.M. 1982. A report on the study of dilation patterns within the Panasqueira ore body: Barroca Grande, Beralt Tin Wolfram (Portugal), unpub. rept.15p.

Hedenquist, J.W., Lowenstern, J.B. 1994. The role of magma in the formation of hydrothermal ore deposits. Nature Vol. 370: 519-526.

Henry, D.J., Guidotti, C.V. 1985. Tourmaline as a petrogenetic indicator mineral: an example from the staurolite-grade metapelites of NW Maine. Am. Mineral. 70,1–15.

Henry, D.H., Dutrow B. L. 1996. Metamorphic tourmaline and its petrologic applications. Reviews in Mineralogy and Geochemistry 33 (1): 503-557.

Ingebritsen, S.E., Manning, C.E. 1999. Geologic implications of a permeability–depth curve for continental crust. Geology 27, 1107–1110.

Ingebritsen, S.E., Appold, M.S. 2012. The physical hydrogeology for ore deposits. Econ Geol 107:559–584

Julivert, M., Fontboté, J.M., Ribeiro, A., Conde, L. 1972. Mapa Tectonico de la Peninsula Iberica y Baleares E. 1:1.000.000. Inst. Geol. Min. España, Madrid.

Kelly, W.C., Rye, R.O. 1979. Geologic, fluid inclusion and stable isotope studies of the tin-tungsten deposits of Panasqueira, Portugal. Econ Geol 74:1721–1822

Kessler, S.E., Stoiber, R.E. & Billings, G.K. 1972. Direction of flow mineralizing solutions at Pine Point, N.W. T., Econ. Geol., **67,** 19–24.

Lecumberri-Sanchez, P., Vieira, R., Heinrich, C.A., Pinto, F., Wälle, M. 2017. Fluid-rock interaction is decisive for the formation of tungsten deposits. Geology 45, 579‑582.

Mahjoubi, E.M., Chauvet, A., Badra, L., Sizaret, S., Barbanson, L., El Maz1, A., Chen, Y., and Amann, M. 2016. Structural, mineralogical, and paleoflow velocity constraints on Hercynian tin mineralization: the Achmmach prospect of the Moroccan Central Massif. Miner. Deposita 51: 431.

Marks, M. A. W., Schühle, P., Guth, A., Wenzel, T. and Markl, G. 2013. Trace element systematics of tourmaline in pegmatitic and hydrothermal systems from the Variscan Schwarzwald (Germany) : the importance of major element composition, sector zoning, and fluid or melt composition. Chemical geology, Vol. 344, p.73-90.

Martinez Catalan, J.R., Arenas, R., Diaz Garcia, F., et al. 2007. Space and time in the tectonic evolution of the northwestern Iberian Massif: Implications for the Variscan belt. In: Hatcher RD, Carlson MP, McBride JH, Martínez Catalán JR (eds) 4-D Framework of continental crust: Geological Society of America Memoir 200.Geological Society of America, 403–423

Norton, D., Cathles, L.M. 1979. Thermal aspects of ore deposition. In: Barnes, H.L. (Ed.), Geochemistry of Hydrothermal Ore Deposits, second ed. John Wiley and Sons, New York, pp. 611e631.

Parnell, J. 1998. Dating and Duration of Fluid Flow and Fluid–Rock Interaction.: Geological Society Special Publication, 144, 284 pp

Polya, D.A. 1989. Chemistry of the main-stage ore-forming fluids of the Panasqueira WCu(Ag)-Sn deposit, Portugal: implications for models of ore genesis. Econ. Geol. 84, 1134‑1152.

Polya, D.A., Foxford, K.A., Stuart, F., Boyce, A., Fallick, A.E. 2000. Evolution and paragenetic context of low δD hydrothermal fluids from the Panasqueira W-Sn deposit, Portugal: New evidence from microthermometric, stable isotope, noble gas and halogen analyses of primary fluid inclusions. Geochim. Cosmochim. Acta 64, 3357‑3371.

Robb, L. 2005. Introduction to Ore-forming Processes. Blackwell Publishing, Malden, MA, 373 p.

Sams, M. S. & Thomas-Betts, A. 1988. Models of convective fluid flow and mineralization in Southwest England. Journal of the Geological Society. 145, 809-817.

Shcherba, G. N. 1970. Greisens. Int Geol Rev 12: 114–255

Sibson, R.H. 1992. Implications of fault-valve behaviour for rupture nucleation and recurrence. Tectonophysics, 211, 283–93.

Sizaret, S., Fedioun, I., Barbanson, L., Chen, Y. 2006. Crystallization in flow part II: modelling crystal growth kinetics controlled by boundary layer thickness. Geophys J Int 167:1027–1034

Sizaret, S., Branquet, Y., Gloaguen, E., Chauvet, A., Barbanson, L., Chen, Y. 2009. Estimating the local paleo-fluid flow velocity: new textural method and application to metasomatism. Earth Planet Sci Lett 280:71–82.

Snee, L.W., Sutter, J.F., Kelly, W.C. 1988. Thermochronology of economic mineral deposits; dating the stages of mineralization at Panasqueira, Portugal, by high-precision 40Ar/39Ar age spectrum techniques on muscovite. Econ Geol 83:335–354

Thadeu, D. 1951. Geologia do couto mineiro da Panasqueira. Comunic Serv Geol Port 32:5–64.

Van Hinsberg, V.J., Henry, D.J., Dutrow, B.L. 2011a. Tourmaline as a Petrologic Forensic Mineral: A Unique Recorder of Its Geologic Past. Elements 7, 327–332.

Van Hinsberg, V.J., Franz, G. and Wood, B.J. 2017. Determining subduction-zone fluid composition using a tourmaline mineral probe. Geochemical Perspectives Letters v3, n1.

Weis, P. 2015. The dynamic interplay between saline fluid flow and rock permeability in magmatic-hydrothermal systems. Geofluids, 15, 350-371.

Whitney, D.L, Evans, B.W. 2010. Abbreviations for names of rock-forming minerals. Am. Mineral 95:185-187.